PERFORMANCE EVALUATION OF OSEM FOR BONE SPECT IMAGING

SURACHAI NGAMRATANAPAIBOON

A THESIS SUBMITTED IN PARTIAL FULFILLMENT
OF THE REQUIREMENTS FOR
THE DEGREE OF MASTER OF ENGINEERING
(BIOMEDICAL ENGINEERING)
FACULTY OF GRADUATE STUDIES
MAHIDOL UNIVERSITY
2004

ISBN 974-04-5444-5

Thesis
Entitled

PERFORMANCE EVALUATION OF OSEM FOR BONE SPECT IMAGING

Surachai Ngamratanapaiboon

Mr. Surachai Ngamratanapaiboon
Candidate

Chiraporn Tochareonchai

Assist.Prof.Chiraporn Tochareonchai,
Ph.D. (Biomedical Engineering)
Major-advisor

Chatchai Neatpisarnvanit

Assist.Prof.Chatchai Neatpisarnvanit,
Ph.D. (Electrical Engineering)
Co-advisor

Rassmidara Hoonsawat

Assoc.Prof.Rassmidara Hoonsawat
Ph.D.
Dean
Faculty of Graduate Studies

Theeraporn Rubcumintara

Assist.Prof.Theeraporn Rubcumintara
Ph.D. (Materials)
Chair
Master of Engineering
Biomedical Engineering Program
Faculty of Engineering

Thesis
Entitled

PERFORMANCE EVALUATION OF OSEM FOR BONE SPECT IMAGING

was submitted to the Faculty of Graduate Studies, Mahidol University
for the Degree of Master of Engineering (Biomedical Engineering)
on
December 2, 2004

Surachai Ngamratanapaiboon

Mr. Surachai Ngamratanapaiboon
Candidate

Assist. Prof. Chatchai Neatpisarnvanit,
Ph.D.(Electrical Engineering)
Member

Assit.Prof. Chiraporn Tochareonchai,
Ph.D.(Biomedical Engineering)
Chair

Assoc. Prof. Pawana Pusuwan,
M.D. Thai Board of Radiology
Member

Assist.Prof.Udom Thipayamontri,
Ph.D. (Physiology)
Member

Assoc.Prof.Rassmidara Hoonsawat
Ph.D.
Dean
Faculty of Graduate Studies
Mahidol University

Assist. Prof. Piya Rattanasuwan
M.Eng.
Dean
Faculty of Engineering
Mahidol University

ACKNOWLEDGEMENTS

I am grateful to Assist. Prof. Chiraporn Tochareonchai, my principal supervisor, for her guidance, precious advice and encouragement throughout. She was always nice and kind when she suggested anything to me. I also would like to thank Assist. Prof. Chatchai Neatpisarnvanit my co-advisor for his comments. I appreciate to Prof. Benjamin M. W. Tsui, Department of Radiology and Radiological Science, Johns Hopkins University, and Prof. Steve R Meikle, Department of PET and Nuclear Medicine, University of Sydney and Dr. Philippe Bruyant, Nuclear Medicine Department, University of Massachusetts, for their valued advice and valuable suggestions. I especially appreciate to Dr. David Lalush Department of Biomedical Engineering, North Carolina State University for his program source codes with image reconstruction. I would like to thank Dr. David Fanning, Yung Dong for their suggestion in IDL programming and image format.

I cordinally thank my readers: Assoc. Dr. Pawana Pusuwan, Assoc. Dr. Sutanta Chiewvit, Dr. Pongpija Tuchinda, Pracha Yambangyang, and Patiyut Sririlas. I especially appreciate to Dr. Chulaluk Komontri for her suggestion in data analysis. I am especially indebted to the Department of Radiological Technology, Faculty of Medical Technology, Mahidol University for giving me an opportunity to use laboratory. My appreciation goes to the Division of Nuclear Medicine, Department of Radiology, Faculty of Medicine Siriraj Hospital for supporting me about patients' data. Many thanks also go to my friends Biomed's 3, Biomedical Engineering Program, Faculty of Engineering, Mahidol University.

Lastly, I am grateful to my family for their financial support, their care, and love. The usefulness of this thesis is dedicated to my father, my mother and all the teachers who had taught me.

Surachai Ngamaratanapaiboon

PERFORMANCE EVALUATION OF OSEM FOR BONE SPECT IMAGING

SURACHAI NGAMRATANAPAIBOON 4337540 EGBE/M

M.Eng. (BIOMEDICAL ENGINEERING)

THESIS ADVISORS: CHIRAPORN TOCHAROENCHAI, Ph.D. (BIOMEDICAL ENGINEERING), CHATCHAI NEATPISARNVANIT, Ph.D. (ELECTRICAL ENGINEERING)

ABSTRACT

The aim of this study was to investigate the performance of ordered subset expectation maximization (OSEM) algorithm for bone SPECT imaging. This study was divided into two parts, first, the noise properties of OSEM and the optimal numbers of iteration and subset were investigated using mathematic Zubal brain phantom. Then, the optimal numbers were implemented for bone SPECT images and the image qualities obtained from OSEM and filtered backprojection (FBP) algorithm were compared using preference study. Two nuclear medicine physicians participated in the study. To determine the image noise, variance was used as an index and mean square error (MSE) was used to determine the optimal parameters of OSEM. For preference study, the agreement of two physicians was determined. The results showed that variance increased as a function of number of iteration and subset. The 2 iterations with 6 subsets gave minimum MSE. For preference study, two physicians agreed that the image obtained from OSEM was superior to that from FBP with 65.6 %. In conclusion, the image noise obtained from OSEM iterative reconstruction increased as numbers of iteration and subset. The optimal numbers of iteration and subset were 2 and 6 respectively. Image quality of OSEM was superior to that of FBP for bone SPECT imaging.

KEY WORDS : ORDERED SUBSET EXPECTATION MAXIMIZATION (OSEM) ALGORITHMN/ BONE SPECT/ FILTERED BACKPROJECTION (FBP) ALGORITHM

46 P. ISBN 974-04-5444-5

การประเมินการทำงานของ OSEM เพื่อใช้ในการถ่ายภาพ BONE SPECT
(PERFORMANCE EVALUATION OF OSEM FOR BONE SPECT IMAGING)

สุรชัย งามรัตนไพบูลย์ 4337540 EGBE/M

วศ. ม. (วิศวกรรมชีวการแพทย์)

คณะกรรมการควบคุมวิทยานิพนธ์: จิราภรณ์ โตเจริญชัย, Ph.D. (BIOMEDICAL ENGINEERING), ฉัตรชัย เนตรพิศาลวานิชย์, Ph.D. (ELECTRICAL ENGINEERING)

บทคัดย่อ

จุดประสงค์ของการศึกษานี้คือการศึกษาคุณสมบัติของ ordered subset expectation maximization (OSEM) algorithm ในการถ่ายภาพ bone SPECT การศึกษาแบ่งออกเป็นสองส่วน ส่วนแรกเป็นการศึกษาคุณสมบัติของ noise ที่เกิดจาก OSEM และจำนวน iteration และ subset ที่เหมาะสมของ OSEM โดยใช้หุ่นจำลอง Zubal ส่วนสมอง ต่อจากนั้นค่าที่เหมาะสมจะนำไปใช้ในการสร้างภาพ bone SPECT และคุณภาพที่ได้จาก OSEM นำมาเปรียบเทียบกับภาพที่ได้จาก FBP โดยใช้แพทย์ด้านเวชศาสตร์นิวเคลียร์ 2 ท่านเป็นผู้ทำการประเมินความพึงพอใจ ในการศึกษาคุณสมบัติของ noise ที่เกิดขึ้นใช้ variance เป็นดัชนี และ mean square error (MSE) ที่น้อยที่สุดนำมาใช้เพื่อหาพารามิเตอร์ที่เหมาะสม จากผลการศึกษาพบว่า noise ที่เกิดขึ้นจะเพิ่มตามจำนวน iteration และจำนวน subset ที่มากขึ้นและจำนวน 2 iteration และ 6 subset ที่ให้ค่า MSE ที่น้อยที่สุด ในการศึกษาความพึงพอใจต่อคุณภาพของภาพ พบว่าผู้ทำการทดสอบพึงพอใจต่อภาพที่ได้จาก OSEM 65.6 % สรุป noise ที่เกิดจาก OSEM algorithm ที่เพิ่มขึ้น ตามจำนวน iteration และ subset จำนวน iteration และ subset ที่เหมาะสมคือ 2 และ 6 ตามลำดับ คุณภาพของภาพที่ได้จาก OSEM ดีกว่าภาพที่ได้จาก FBP ในการการถ่ายภาพ bone SPECT.

46 หน้า. ISBN 974-04-5444-5

CONTENTS

CONTENTS (Continued)

LIST OF TABLES

LIST OF FIGURES

LIST OF FIGURES (Continued)

LIST OF ABBREVIATIONS

FBP	Filtered backprojection
GUI	Graphic user interface
IDL	Interactive data language
IDLE	Interactive data language environment
PHA	Pulse height analyzer
PMT	Photomultiplier tube
MLEM	Maximum likelihood expectation maximization
MRI	Magnetic resonance imaging
MSE	Mean square error
OSEM	Ordered subset expectation maximization
ROI	Region of interest
SPECT	Single photon emission computed tomography

CHAPTER I
INTRODUCTION

Nuclear medicine is a medical specialty that uses safe, painless and cost effective techniques both to image the body and to treat disease. Nuclear medicine imaging also called emission imaging is unique in that it documents organ function and structure, in contrast to diagnostic radiology, which is based upon anatomy as shown in Figure 1.1 (1, 2). To form the image, photons in the patients are emitted in all directions and detected. Nuclear medicine imaging instruments mostly use scintillation detectors. Single photon emission computed tomography (SPECT) is one of the two forms of emission tomography: SPECT and Positron Emission Tomography (PET). It generates transverse images of the organ by acquiring a number of 2D projection data around the patient and then reconstructed.

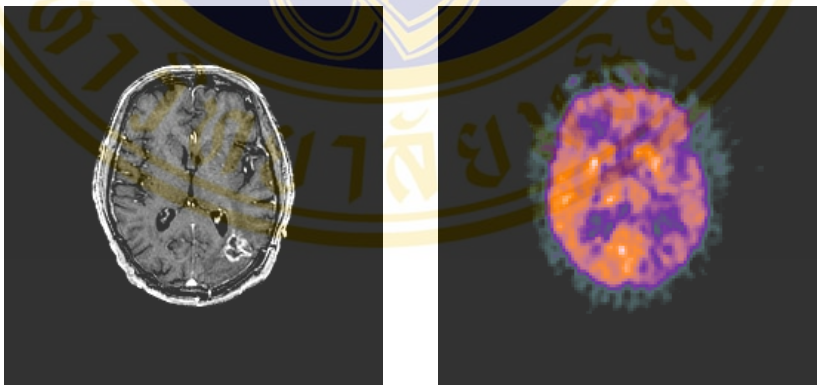

(a) (b)

Figure 1.1 The same slice of the brain images obtained from MRI (a) and SPECT (b). (3)

Most commonly used image reconstruction methods in nuclear medicine are analytical and iterative. The analytical methods are based on exact mathematical solutions to calculate radioactivity distribution from the projections. The most popular analytical method is filtered backprojection algorithm (FBP). This algorithm is based

on direct inversion of the Radon transform (4). The limited number of projection data sets introduced streak artifact in the reconstructed images as shown in Figure 1.2. Moreover, it is very difficult to compensate for image degrading factors using this algorithm. Despite its drawbacks, FBP is used extensively in nuclear medicine because it is robust and fast.

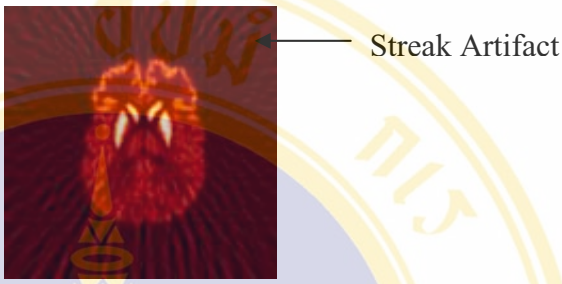

Figure 1.2 SPECT brain with streak artifact (arrow).

In clinical study, streak artifacts obtained from FBP algorithm degrade SPECT image quality and then ones attempts to improve it. Iterative reconstruction methods have been introduced and a major advantage of this method is the possibility of incorporating compensation for image degrading factors. There are different iterative algorithms some based on the methodologies of numberic linear algebra and others based on statistical approaches. The latter method has been recently used in nuclear medicine and the most popular algorithm is ordered subset expectation maximization (OSEM), because it allows us to improve image quality and accelerates the reconstruction time. Several studies show the advantage of OSEM over FBP (5, 6, 7, 8, 9, 11, and 12)

Bone scan evaluates bone physiological and skeleton anatomy and bone SPECT improved sensitivity and anatomy details in 3D format. As a result, the sites of abnormalities gave the information about the diseases leading to the appropriate treatments. Therefore, image quality of bone SPECT obtained from OSEM is of interest.

In this study, we developed an iterative reconstruction; OSEM algorithm using IDL language for improving image quality of Bone SPECT. The noise properties of OSEM and optimal parameters for bone SPECT images were investigated.

CHAPTER II
OBJECTIVES

This research aims at studying the performance of OSEM for bone SPECT imaging as follows:

1. To study the noise properties of OSEM algorithm as a function of numbers of iteration and subset.
2. To determine the optimal parameters of OSEM algorithm such as numbers of iteration and subset.
3. To compare image quality obtained from OSEM algorithm and that from filtered backprojection (FBP) algorithm using a preference study.

CHAPTER III
BACKGROUND

3.1 Single Photon Emission Computed Tomography (SPECT)

Single photon emission tomography (SPECT) is used to generate transverse images depicting the distribution of photon emitting nuclide in-patients. Projection images or sinograms are acquired from different views around the patients. SPECT systems use one or more scintillation camera heads that rotate around the patients as shown in Figure 3.1. SPECT is particularly useful and significantly improves clinical results because individual tomographic planes or slices are physically distinguished and nonoverlapping. SPECT also provides high signal-to-noise ratio as well as accurate representation of the actual activity distribution, which is of importance for quantitative nuclear medicine studies (1).

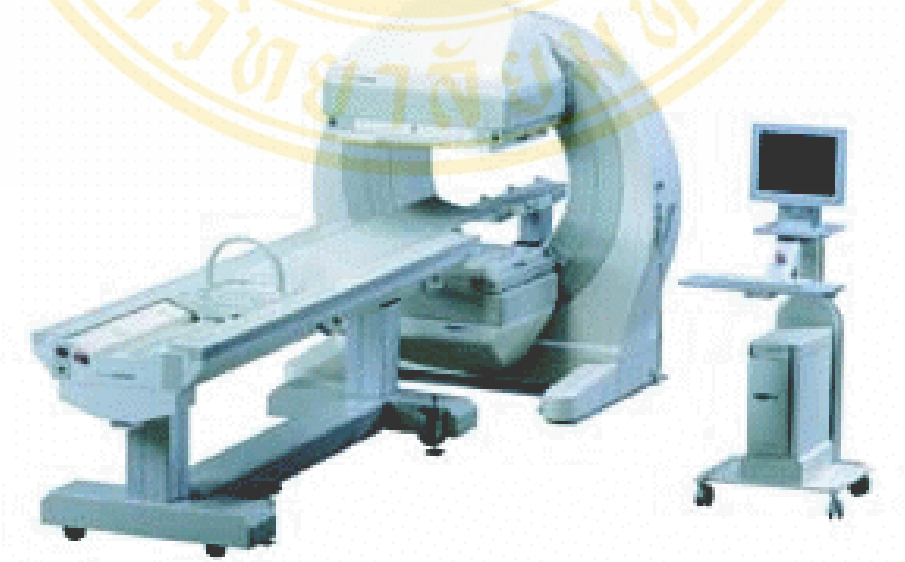

Figure 3.1 SPECT systems (13).

3.1.1 System Configuration

A scintillation camera illustrated in Figure 3.2, contains a disk-shaped or rectangular thallium activated sodium iodide NaI(Tl) crystal, typically 0.95 cm thick, optically coupled to a large number (typically 37 to 91) of 5.1 to 7.6 cm diameter photomultiplier tubes (PMTs). In most cameras, a preamplifier is connected to the output of each PMT. Some camera designs incorporate a Lucite light-pipe between the glass cover of the crystal and PMTs; in others, the PMTs are directly coupled to the glass cover. Between the patient and crystal is a collimator, usually made of lead, which only allows x- or gamma rays approaching from certain directions to reach the crystal. The pulses from the individual preamps after each x- or gamma ray interaction in the crystal and, by determining the centroid of these pulses produced an x-position and y-position pulses that together specified the position of the interaction in the plane of the crystal. The summing circuit adds the pulses from the individual preamp to produce energy (z) pulse proportional in amplitude to the total energy deposited in the crystal. The z-pulse from the summing circuit is sent to a pulse height analyzer (PHA). When the pulse falls within the selected energy window the x- and y-position pulses are then sent to display on cathode ray tube corresponding to the location at which the scintillation event occurred in the crystal (14).

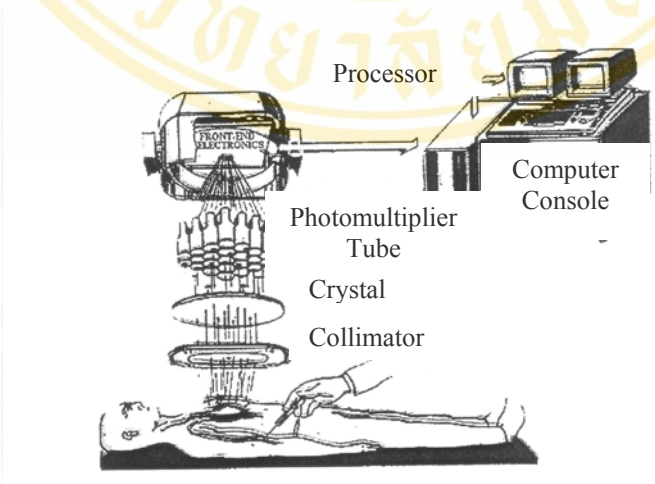

Figure 3.2 Basic components of scintillation detector. The scintillation detector consists of collimators, sodium iodide crystal, photomultiplier tubes and electrical circuits (14).

3.1.2 Data Acquisition

To acquire the data, the detector or camera rotates around the patients and images at uniform angular increments are obtained on the basic of its location. The z-axis is assigned to be the axis of rotation of the camera. The size of the sampling interval is called picture element (pixel) or voxel and the locations on the camera face are divided into discrete elements called projection bins.

- Line Integrals and Projections

A line integral represents the summation of the radioactivity or counts of the object along a given direction and the collection of all line integrals parallel to a given direction is called a projection. Figure 3.3 shows the projection images of the patient at different angles. Sinogram as shown in Figure 3.4 is related to the projection image. In the sinogram, the data at the same row (dotted line) from all the projection images is redisplayed. The vertical axis represents the projection angle or view and the horizontal axis represents the projection bin or number of image pixel.

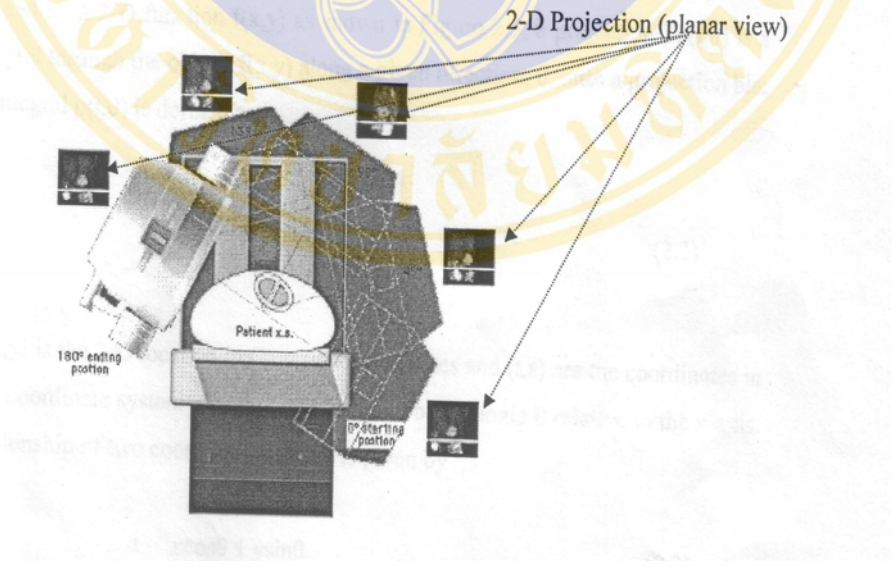

Figure 3.3 Illustration of projection images of the patient at different angles (15).

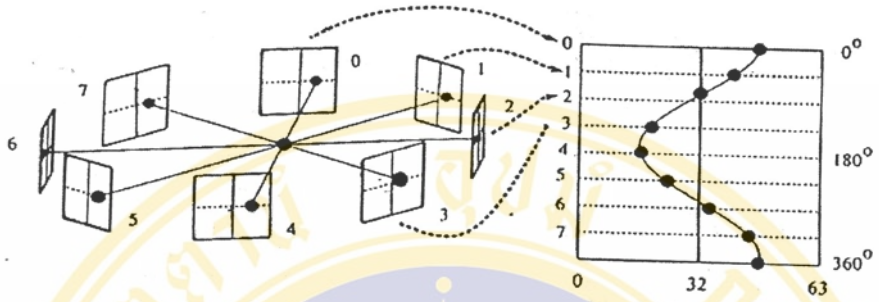

Figure 3.4 Illustration of sinogram which is related to the projection image. The vertical axis represents the projection angle or view and the horizontal axis represents the projection bin or number of image pixel (16).

To describe line integrals and projections, the object as shown in Figure 3.5 is represented by a 2D function, $f(x,y)$, a projection, $p(t,\theta)$, is a line integral through the object, $f(x,y)$, along a given direction, θ, onto a projection bin, t. Line integral $p(t,\theta)$ is defined as

$$p(t,\theta) = \int_{-\infty}^{+\infty} f(x,y)ds \qquad (3.1)$$

where (x,y) is the 2D location in Cartesian coordinates and (t,s) are the coordinates in a related coordinate system where t-axis is rotated by an angle θ relative to the x-axis. The relationship of two coordinate systems is given by

$$t = x\cos\theta + y\sin\theta \qquad (3.2)$$

$$s = -x\sin\theta + y\cos\theta \qquad (3.3)$$

The function $p(t,\theta)$ is known as the Radon transform of the function $f(x,y)$ (4).

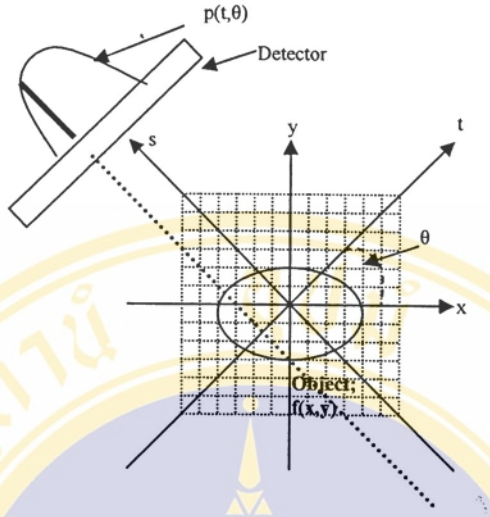

Figure 3.5 The projection $p(t,\theta)$ is the line integral of the radioactivity in a dotted line (ray) across the object.

3.1.3 Image Reconstruction from Projections

There are two classes of image reconstruction methods used in SPECT, analytical and iterative. The analytical reconstruction is based on discrete implementations of analytical of the inverse Radon transform problem. Iterative methods attempt to estimate the object distribution by using iterative technique. This method consists of an underlying statistical model, an iterative algorithm and a projector/backprojector pair. An advantage of iterative methods is the ability to incorporate detector response, attenuation and scatter in to the reconstruction process (17).

- Filtered Backprojection (FBP)

The most widely used analytical reconstruction method in SPECT imaging is filtered backprojection (FBP). The concept of this algorithm is that the object $f(x,y)$ is related to its projection by a simple integral (4),

$$f(x,y) = \int_0^{\pi} p_f(t,\theta)d\theta \qquad (3.4)$$

where p_f is a filtered version of the projection acquired at angle θ. This algorithm as illustrated in Figure 3.6 as follows (16):

1. take the 1D Fourier transform (FT) of a projection $p(t,\theta)$,
2. filter the FT of the projection , $P(v_{t,}\theta)$, by multiplying a filter function,
3. inverse FT of the filtered projection, $p_f(t,\theta)$,
4. backproject the filtered projection on to the image plane, and
5. repeat steps 1 – 4 for all projections.

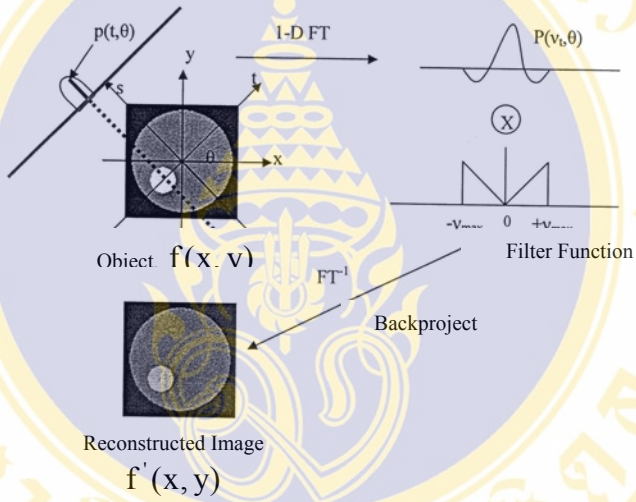

Figure 3.6 Filtered backprojection reconstruction methods. First, the projection data, $p(t,\theta)$ obtained from the object, $f(x,y)$, are transformed into the frequency domain using 1D Fourier transform (FT). Next, the FT of data is multiplied by a filter function and then the inverse Fourier transform (FT^{-1}) of the filtered FT data is taken. Finally, the FT^{-1} projection data is backprojected. After repeating all the steps for all projections, the reconstructed image is created, $f'(x,y)$.

This algorithm is simple and fast. However, FBP does not work well in the clinic, one of the problems is insufficient projection data causing streak artifact in the SPECT image as shown in Figure 1.2. It is also difficult to implement compensations for image degrading factors. This algorithm is derived assuming that the projection

data are ideal, i.e., not affected by degrading factors such as noise, attenuation, detector response or scatter (4, 16).

- Ordered Subset Expectation Maximization (OSEM)

Iterative methods are contrast to analytical ones. Iterative methods attempt to refine estimates of f(x,y), rather than arriving at an estimate by direct inversion of the image transform. These methods allow a more accurate modality of the data acquisition than the line integral modal. Moreover, the advantage of iterative methods is the ability to incorporate priori information about the image into reconstruction process. As a result, the image quality is improved (17).

The principle of the iterative algorithm as shown in below diagram is to find a solution by successive estimates. The projections corresponding to the current estimate are compared with the measured projections. The result of the comparison is used to modify the current estimate, thereby creating a new estimate. The algorithms differ in the way the measured and estimated projections are compared and the kind of correction applied to the current estimate (4).

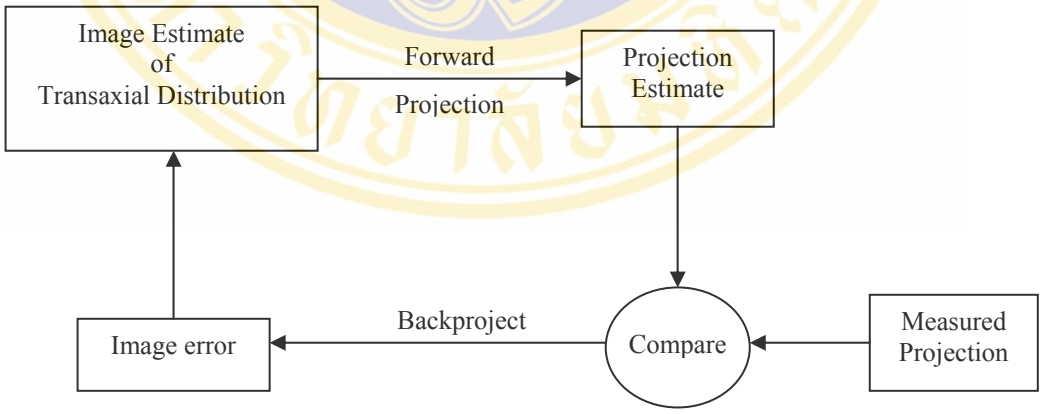

After Hudson and Larkin presented the ordered-subset expectation maximization (OSEM) algorithm, it has been used extensively in SPECT image reconstruction, primarily because of the following reasons (4, 16, 17, 18)

- It provides better image quality, quantitative accuracy and reduces image artifacts as compared with conventional reconstruction methods.
- It converges quickly.
- It is easily implemented with any type of system model.

Since the OSEM results from a modification of maximum likelihood expectation maximization (MLEM) algorithm, the explanation of OSEM algorithm may start from MLEM algorithm.

MLEM assumes that measurements are subject to variations due to the Poisson probabilistic phenomena of the radioactive disintegration. The goal of the MLEM is to find a general solution as the best estimate for the pixel value in the image (x_i): The mean number of radioactive disintegration in the image that can produce the sinogram or projection p_j with the highest likelihood. This can be done using the Poisson law that allows one to predict the probability of a realized number of detected counts, given the mean number of disintegrations. Thus, each iteration is divided in 2 steps: in the expectation step (E step), the formula expressing the likelihood of any reconstructed image given the measured data is formed, and in the maximization step (M step), the image that has the greatest likelihood to give the measured data is found (4). The MLEM algorithm can be written as (18)

$$x_j^{k+1} = \frac{x_j^k}{\sum_{i=1}^{n} a_{ij}} \sum_{i=1}^{n} \frac{p_j}{\sum_{j}^{m} a_{ij'} x_j^k} a_{ij} \qquad (3.5)$$

where x_i represents the estimated counts at pixel i, and p_j is the measured data in projection bin j. The a, called transfer matrix, contains all the information about the imaging process. The factor $\frac{p_j}{\sum_{j}^{m} a_{ij} x_j^k}$ is the ratio of the measured projection p_j to the

current estimate projection ($\sum_{j}^{m} a_{ij} x_j^k$). This factor is then backprojectected and normalized by $\frac{1}{\sum a_{ij}}$.

In other words, at each iteration a current estimate of the image is available. The projection estimates are calculated and then the measured projections are compared with projection estimates. The ratio is used to modify the current estimate to generate an updated image estimate. This process is repeated many times.

In OSEM algorithm, the set of measured projections is divided into subsets (or blocks), and then MLEM is applied to each subset in turn, as a sub-iteration. The first full iteration is complete when all subsets have been processed. The OSEM can be written as (19)

$$x_j^{k+1} = \frac{x_j^k}{\sum_{j \in S_n}^{n} a_{ji}} \sum_{j \in S_n}^{n} \frac{p_j}{\sum_{j}^{m} a_{ij} x_j^k} a_{ij} . \qquad (3.6)$$

where S_n is a subset of the projection bins j.

For example, if there are 64 projections and they are divided into 4 subsets, each containing 16 projections. The algorithm will start with the first subset, as follows:

1. The initial image estimate is generated.
2. The 16 projection estimates of the initial image estimate are calculated.
3. The ratios of measured projections to the projection estimates are calculated and then summed to obtain the projection error.
4. The projection error is backprojected to get the image error.
5. Finally, the initial image estimate is updated by the image error.
6. Use the update image estimated for the next subsets.
7. Repeat from step 2-6 until all the subsets have been processed. That is the end of the full iteration.
8. For the next iteration, repeat step 2-7 until criterion is met.

3.2 Image Quality Assessment

Image quality and clarity generally refer to the degree of visibility of relevant information in an image. The assessment of image quality may be done subjectively or objectively. It may involve the detection (human observers) or estimation tasks (using mathematics models)

Image noise is one of the fundamental physical parameters (spatial resolution, contrast and noise) for the estimation task. It is also complicated in the tomographic images because it is a function of both the reconstruction method and the projection data used to create the image (20).

To study the noise properties of iterative reconstruction methods, noise variance and mean square error (MSE) are commonly used as image quality indices (10, 21). The noise variance over the region of interest (ROI) in the reconstructed image is defined as

$$\text{Variance} = \frac{1}{N^2}\sum_{i=1}^{N}(x_i^R - \bar{x})^2 \qquad (3.7)$$

where x_i^R is i^{th} pixel value of the reconstructed image, $\bar{x}$ is mean value of the reconstructed image and N is number of pixel.

The mean square error measures the differences over the ROI between a reconstructed image and the truth image (10). It is defined as follows

$$\text{MSE} = \frac{1}{N}\sum_{i=1}^{N}(x_i^T - x_i^R)^2 \qquad (3.8)$$

where x_i^T and x_i^R are i^{th} pixel value of the reconstructed image and the truth image. N is number of pixel.

Although estimation task is attractive and plays a critical role in quantitative image analysis, it is not corrected with human assessment of images.

3.3 Interactive Data Language (IDL) (22, 23)

The Interactive data Language (IDL) was designed and developed in the early 1970s for researchers who wanted to extract results from their data quickly and with minimal programming while maintaining control of their data throughout processing. IDL is popularly used in many fields, such as medical, engineering.

IDL is a complete, structured language that can be used interactively, sophisticated functions, procedures and applications. It is flexible input/output facilities allow user to read any type of custom data format. Its programs run the same across all supported platforms (UNIX, VMS, Microsoft windows and Macintosh system) with little or no modification. Another IDL widget tool kit application can be used to quickly create multi-platform graphic user interface to programs.

3.3.1 IDL Development Environment (IDLDE)

IDLDE is a conventional graphic user interface that includes built-in editing and debugging tools. This section describes briefly IDLDE for more detail can read from reference 22 and 23. There are eight major components as follows.

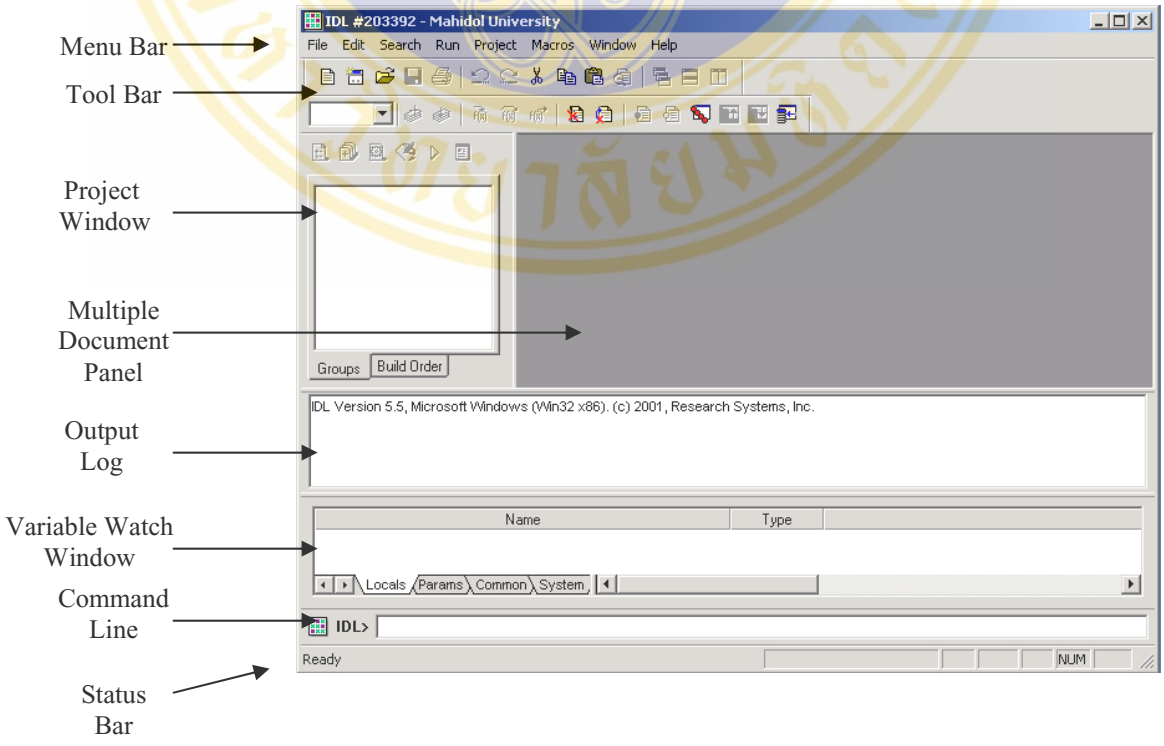

Figure 3.7 The IDL development environment for windows.

- Menu Bar

It is located at the top of the main IDL window that is used to control various IDLDE features.

- Toolbar

IDLDE contains three tool bars that are Standard, Run and Debug, and Macros.

- Project Window

The Project window shows information about the current project which has opened. IDL Projects allows user to easily develop application in IDL. User can manage, compile, run, and create distributions of all the files you will need to develop IDL application.

- Multiple Document Panel

This part displays IDL Editor Window where user create application as shown in Figure 3.8.

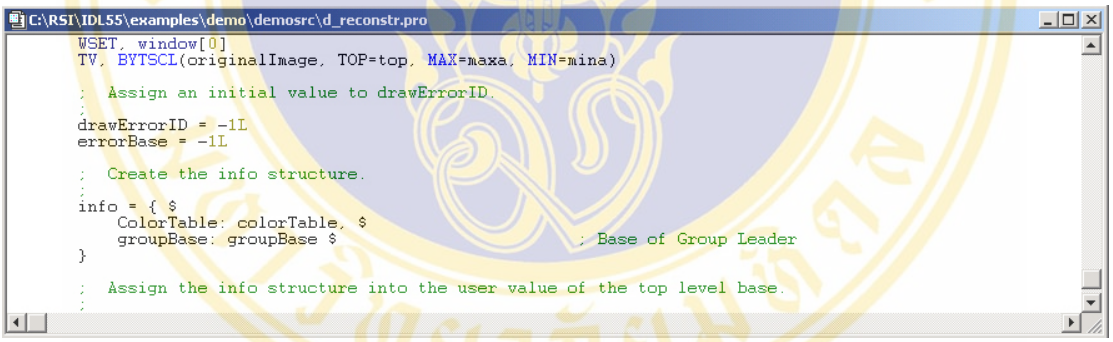

Figure 3.8 Editor Windows

- Command Line

It is a single IDL prompt where user can enter IDL commands.

- Output Log

Output from IDL is shown in the Output Log window that appears by default when the IDLDE is started.

- Variable Watch Window

The Variable Watch window keeps track of variables as they appear and change during program execution.

- Status Bar

When user position the mouse pointer over a Control Panel button or select an option from a menu item in the IDLDE, the Status Bar displays a brief description.

3.3.2 Graphic User Interfaces Programming in IDL

Graphic user interfaces (GUIs) provide a point-and-click way to run applications in a windowed environment. Complex and repetitive tasks can often be simplified by an interactive GUI, which hides the implementation details and allows the user to focus on completing the task. IDL provides a built-in GUI development toolkit, which allows user to build the applications on any IDL platform. For example, the SPECT image reconstruction includes an application built entirely with the GUI tool kit that demonstrates image reconstruction tool capabilities as shown in Figure 3.9.

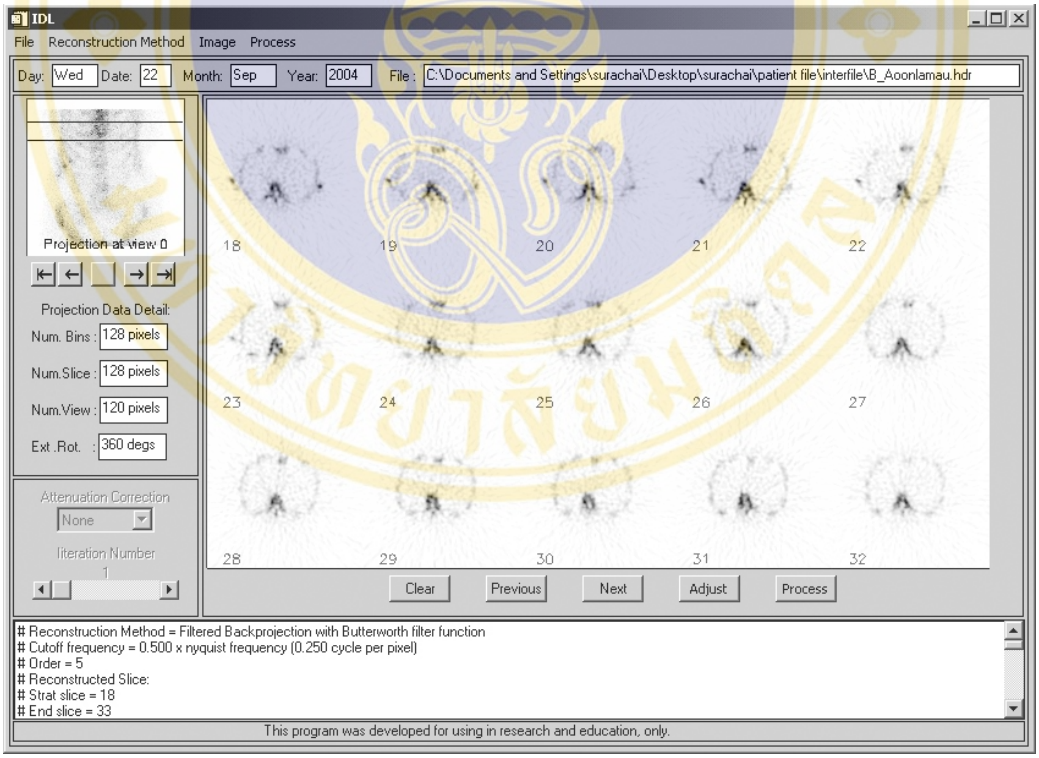

Figure 3.9 Graphic user interface of image reconstruction tool demonstration

This section introduces the concepts necessary to build IDL applications with GUIs and theirs components. This section continues with an in-depth explanation of the functions used to create GUI using widget tool kit.

- GUI Components (Widgets)

A GUI application typically consists of a variety of a component called widgets. Each widget has a particular appearance, and the application responds in a certain way when the widget is interacted. There are nine fundamental widget types available in IDL as shown in Table 3.1.

Table 3.1 Widget fundamental types.

Widget	Description
Base	Container for other widgets
Button	Clickable button
Draw	Graphics window
Droplist	Button that drops to reveal a selectable list
Label	Noneditable label
List	List of selectable items, often with scrollbars
Slider	Horizontal or vertical slider
Table	Editable
Text	Editable text field

- Creating Widgets

The first widget created in a GUI must be a base because a base is required to contain all the widgets subsequently created inside the GUI. This base is known as a top-label base or parent widgets, which is a parent to all the widgets contained within it. Widgets contain within the parent widget called child widgets. The widget-child relationship can be illustrated in Figure 3.10.

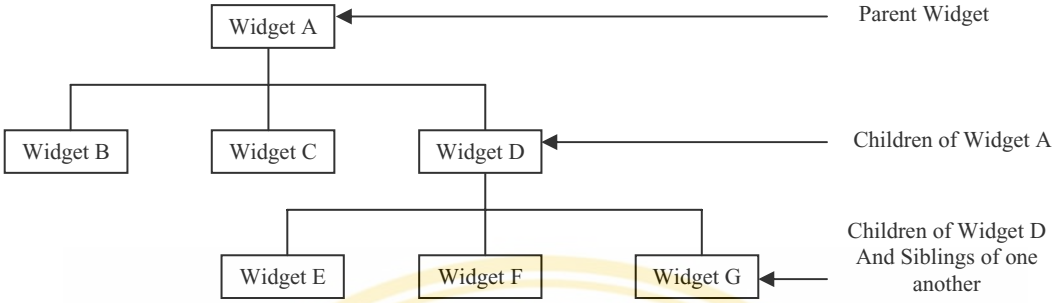

Figure 3.10 A diagram of a widget hierarchy. Widget A is a parent widget and is the container that holds all the other widgets. Widget B, C, and D are child widgets of widget A. Widget F, G and H are children of widget D.

The creating widget functions can be summarized in Table 3.2. The more detail can be read from reference (22).

Table 3.2 Fundamental Widget Creation

Widget	Function
Base	id = widget_base([parent], [keyword])
Button	id = widget_button(parent, [keyword])
Draw	id = widget_draw(parent, [keyword])
Droplist	id = widget_droplist(parent, [keyword])
Label	id = widget_label(parent, [keyword])
List	id = widget_list(parent, [keyword])
Slider	id = widget_slider(parent, [keyword])
Table	id = widget_table(parent, [keyword])
Text	id = widget_text(parent, [keyword])

3.4 Reconstruction Tool Development

The program, being developed in this thesis, features image reconstruction function from projection data. This section contains the basic features of the developed program with interface samples.

3.4.1 Main Menu Graphic User Interface (GUI)

After running the program, the main menu will be display on the screen as shown in Figure 3.11.

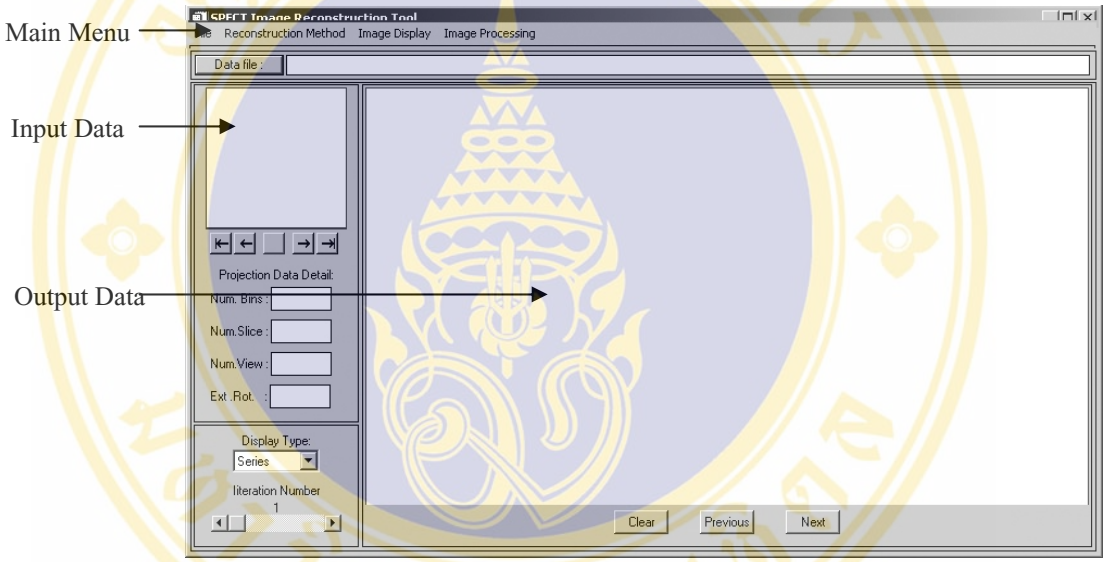

Figure 3.11 Display windows.

The upper region consists of options such as ‘File’, ‘Reconstruction method’, ‘Display’, and ‘Processing’

- ‘File’

This option is used to open or import projection data for reconstruction. The file formats used in this program are interfile and DICOM. This function is capable of three dimensional data (number of bins, slices and views) and display in CINE mode. This option has 4 submenus such as import, export, file info and exit as shown in Figure 3.12

Figure 3.12 File menu.

- 'Reconstruction Method'

This option has two submenus: FBP and OSEM. For FBP, there are 5 options to select for image filtering as shown in Figure 3.13.

Figure 3.13 Reconstruction method menu.

- 'Image Display'

This option has fours submenus for output display such as 'Projection', 'Reconstructed Image', 'Volume', and 'Color' as shown in Figure 3.14.

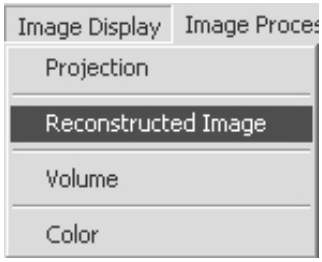

Figure 3.14 Image display menu**.**

- ‘Image Processing’

There are two submenus in this option such as ‘smoothing’ and ‘Enhance’ as shown in Figure 3.15.

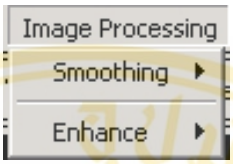

Figure 3.15 Image processing menu**.**

3.4.2 Reconstruction Process Design

This section describes the process of two reconstruction methods (FBP and OSEM) were written. Figure 3.16 and 3.17 show the flow charts of the two methods.

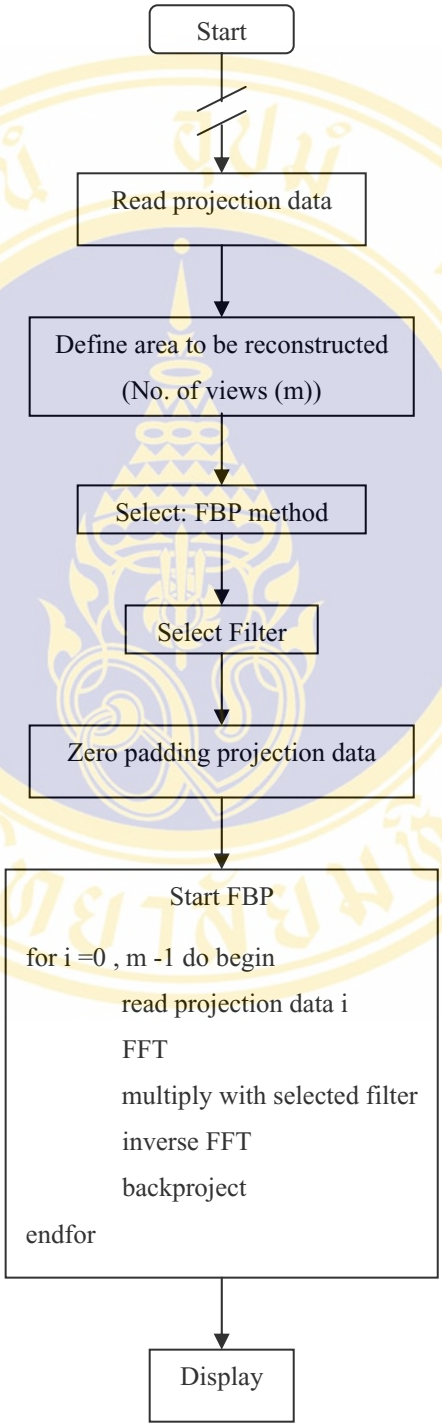

Figure 3.16 Flow diagram of FBP algorithm.

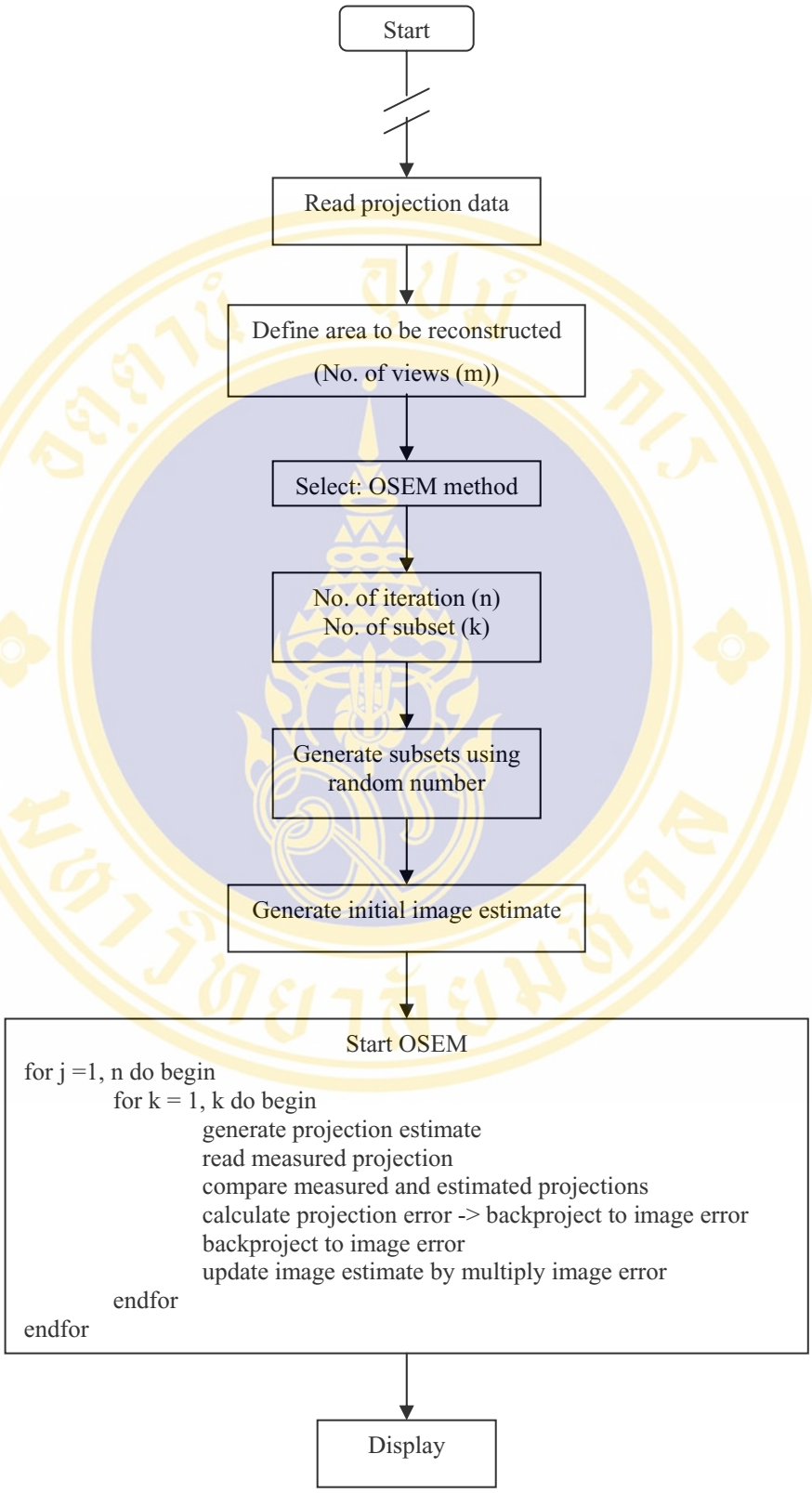

Figure 3.17 Flow diagram of OSEM algorithm.

CHAPTER IV
MATERIALS AND METHODS

This chapter will present the materials and methods used in this thesis. The first part will describe the methods to determine noise properties and optimal subset and iteration number of OSEM. The second part will be preference study that mimics the clinical situation. Readers will select the image reconstruction algorithms that give the best image quality. For image reconstruction software, we used IDL which we developed for this study using IBM PC AMD 2 GB and 348 MB RAM.

4.1 The Study of Noise Properties of OSEM

In this part, the mathematics Zubal brain phantom was used. This phantom was developed by Prof. George Zubal (24) in 1995. It allows users to flexibly design the activity in the brain. In this study, the assigned activities of stratum, frontal lobe, gray and white matters were 75, 45, 35 and 15 respectively. Figure 4.1 shows some slices of Zubal phantom that used in the study.

Figure 4.1 Some slices of Zubal phantom.

4.1.1 Projection Data Generation and Image Reconstruction

We used the software namely “genprj” developed by MIRL group at University of North Carolina at Chapel Hill to generate the projection data of Zubal phantom. Poisson noise and collimator-detector blurred with 5 pixel width of gaussian distribution were added to the projection data. The data set was 128x128 matrix size

with 120 views over 360 degrees, then reconstructed using OSEM algorithm with various subset and iteration numbers. The number of subset ranged from 2 to 30 with increment of 2 and number of iteration ranged from 1 to 30 with increment of 1. The image reconstruction software was developed using IDL version 5.5 on window platform. The reconstruction times of OSEM were not longer than 3.25 sec/slice.

4.1.2 Data Analysis

The reconstructed image which had a uniform distribution of counts was selected for each condition. Then the regions of interest (ROIs) of 5x5 pixels were drawn over the uniform areas as shown in Figure 4.2. The counts in each ROI were recorded and variance was calculated.

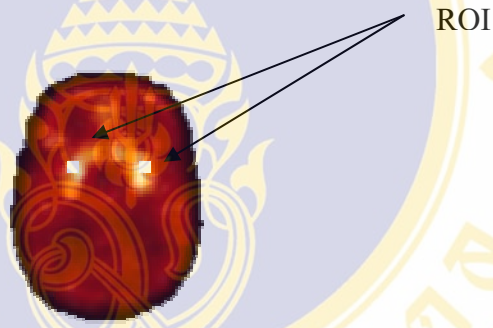

Figure 4.2 Region of interest (ROI) over the reconstructed image.

4.2 The Optimal Subset and Iteration Number of OSEM

The reconstructed images with various subset and iteration number from section 4.1 were used. The true images which were the same cuts of reconstructed images were selected. The data over ROIs of the two sets of images were collected and MSEs were determined. The minimum value of the MSEs was used as an index of the optimal subset and iteration numbers.

4.3 Preference Study

As mentioned before, the single parameter of estimation task for image quality assessment is not related to how physician diagnoses the diseases. In this section, we used the physicians' preference to determine the best image reconstruction algorithm that gives the best image quality.

4.3.1 Data Collection

In this study, thirty-two patients who underwent bone SPECT imaging at Division of Nuclear Medicine, Siriraj Hospital were used. All the patients collected had the symptom of back-bone pain and they were requested to distinguish the source of the pains between bone degeneration and bone metastasis.

4.3.2 Image Reconstruction

Two image reconstruction algorithms (FBP and OSEM) were used. For FBP algorithm, the images were post-filtered using 2D Butterworth (low-pass filter) with 0.25 cycles/pixel cut-off frequency and order 5. For OSEM algorithm, the optimal subset and iteration number obtained from section 4.2 was used and the images were post-filtered using Butterworth (low-pass filter) order 5 and 0.25 cycles/pixel cut-off frequency.

4.3.3 Number of Images

Large numbers of images are required to minimize the error. Then for each patient, 4 images of the suspected areas which caused bone pain were selected. Therefore, 128 images of each image reconstruction algorithm were generated. The images were divided into two groups. Thirty-two images (an image each patient) were used for training and the rest were used for test images.

4.3.4 Image Normalization

For maximizing the image contrast on the monitor display which uses 256-grayscale level, the reconstructed images were normalized to 0-255. First, the maximum count in each image of each reconstruction algorithm was determined, and then scaled to 255. Negative values in the image will be normalized to zero.

4.3.5 Image Display

The displayed images were enlarged to twice their original sizes by bilinear interpolation. The image display scene was divided into 3 regions as shown in Figure 4.3. The upper region showed the instruction on how to select the image and the middle region displayed a pair of reconstructed images which were obtained from FBP (image A) and OSEM (image B). The bottom region was the button to click for selection.

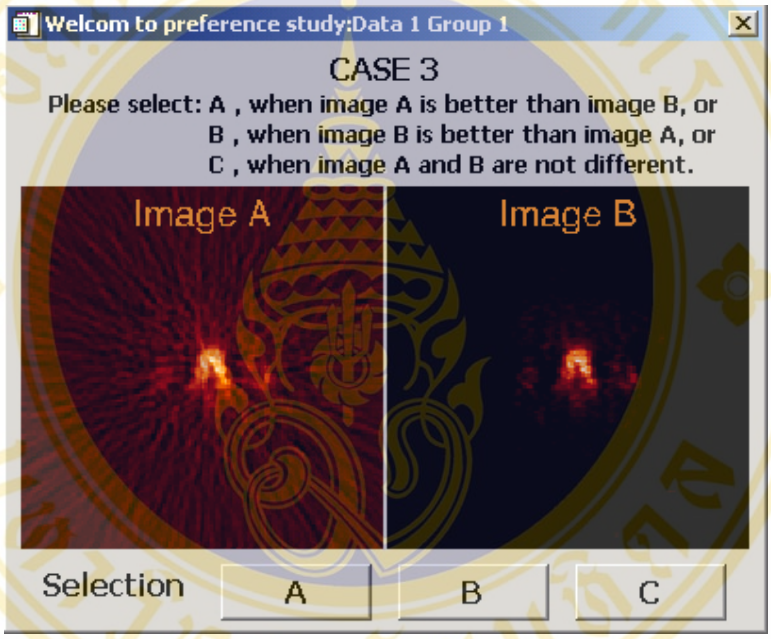

Figure 4.3 Image display format used in the preference study.

4.3.6 Readers

Actually, three nuclear medicine physicians were participated in this study. Unfortunately, one of them did not clearly understand the procedure and did not follow the instruction. As a result, we excluded this reader out of the study.

4.3.7 Task method

At the beginning, the readers read the instructions of the study and were explained the criteria of how to select the reconstruction algorithm which gave the best localization of hot lesion. Without steak artifacts was another criterion if both algorithms were not different for localization. The readers were asked to select one of

the three options; “A” represented the quality of image A better than that of image B and “B” represented the quality of image B better than that of image A. If the image qualities of both algorithms were not different, the readers were asked to select “C”.

The readers were not told the details of the images to avoid prejudges that might impact the results. Due to reader fatigue and time-consuming, 96 test images each algorithm were split into 3 blocks and each block contained 32 images. The readers were told to take their own time to finish the task but they have to finish with in one day.

4.3.8 Data Analysis

The frequencies of the scores obtained from each reader were determined. Individual preference was evaluated and the agreement between two readers was also studied.

CHAPTER V
RESULTS

This chapter presents the results of the study of noise properties of OSEM. The optimal subset and iteration numbers of OSEM are also determined. Finally, the preference study evaluates the image reconstruction algorithm that gives the best image quality for bone SPECT imaging.

5.1 The Study of Noise Properties of OSEM

In this section, the noise properties of OSEM algorithm were determined in term of variance. We studied the variances of reconstructed images over the ROIs of 5x5 pixels. Figure 5.1 and 5.2 show the reconstructed images with different subset and iteration numbers. The variances as functions of numbers of subset and iteration were investigated. Table 5.1 reported the variances with various numbers of subset and iteration. Figure 5.3 demonstrates the increases of average variances when increasing numbers of iteration at different subset numbers. The results showed that the variance increased when the numbers of subset and iteration increased.

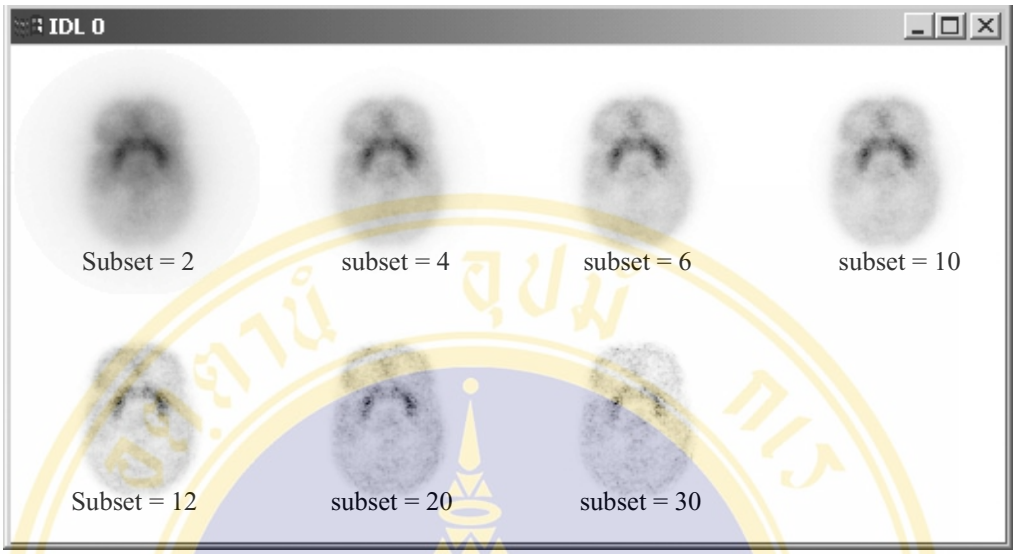

Figure 5.1 Brain phantom images were reconstructed using a single iteration at different numbers of subset.

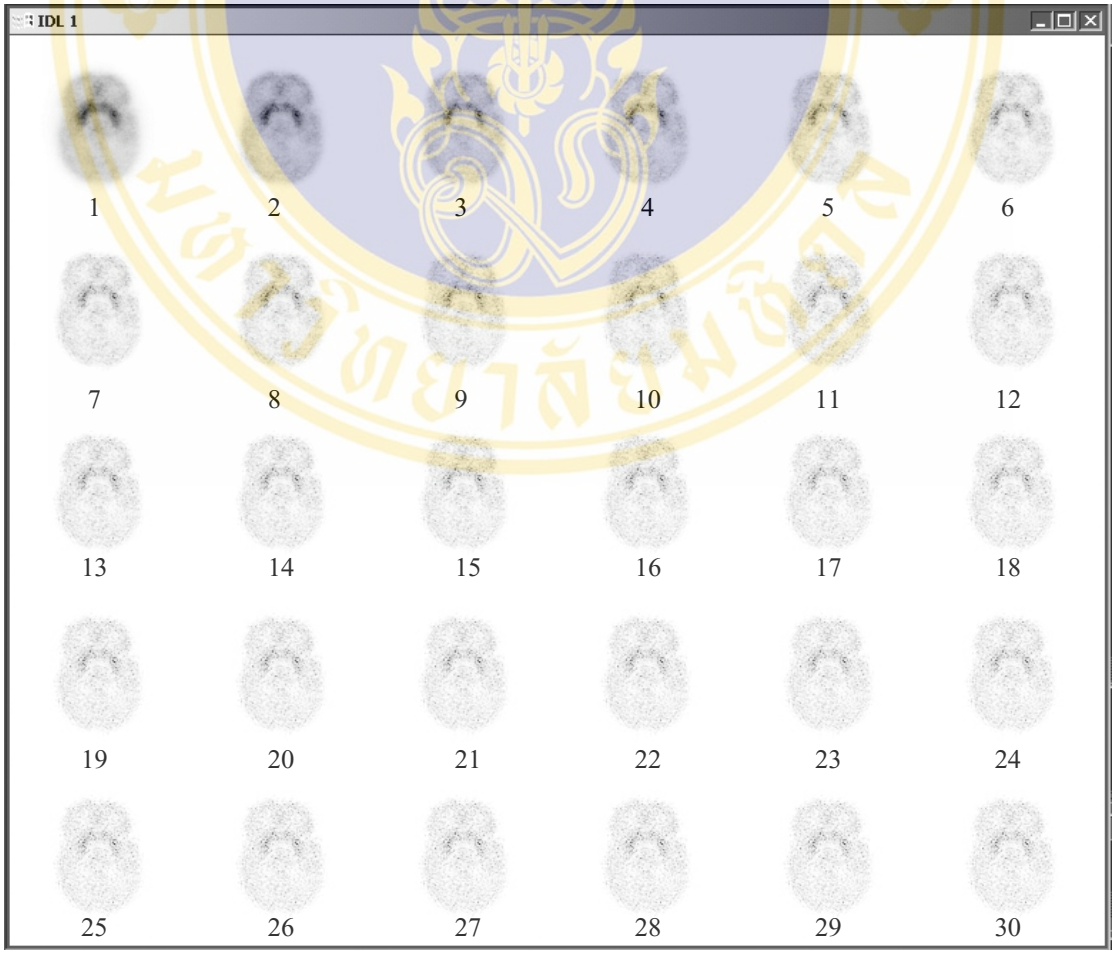

Figure 5.2 Brain phantom images were reconstructed using 6 subsets at different numbers of iteration.

Table 5.1 Variances as a function of numbers of subset and iteration.

Iteration Number	Subset = 2			Subset = 4		
	Left	**Right**	**Average**	**Left**	**Right**	**Average**
1	7.8	8.4	**8.1**	23.0	27.0	**25.0**
2	22.1	27.0	**24.6**	42.3	67.2	**54.7**
3	30.3	44.9	**37.6**	75.7	134.6	**105.1**
4	41.0	67.2	**54.1**	123.2	225.0	**174.1**
5	54.8	98.0	**76.4**	179.6	324.0	**251.8**
6	72.3	134.6	**103.4**	243.4	432.6	**338.0**
7	94.1	176.9	**135.5**	309.8	547.6	**428.7**
8	116.6	225.0	**170.8**	380.3	670.8	**525.5**
9	144.0	275.6	**209.8**	449.4	789.6	**619.5**
10	171.6	327.6	**249.6**	519.8	912.0	**715.9**
11	201.6	380.3	**290.9**	590.5	1036.8	**813.7**
12	234.1	436.8	**335.5**	660.5	1162.8	**911.7**
13	265.7	492.8	**379.3**	729.0	1288.8	**1008.9**
14	299.3	552.3	**425.8**	795.2	1413.8	**1104.5**
15	334.9	610.1	**472.5**	858.5	1536.6	**1197.6**
16	368.6	670.8	**519.7**	924.2	1664.6	**1294.4**
17	404.0	729.0	**566.5**	992.3	1780.8	**1386.5**
18	436.8	789.6	**613.2**	1049.8	1901.0	**1475.4**
19	470.9	852.6	**661.8**	1115.6	2016.0	**1565.8**
20	506.3	912.0	**709.1**	1169.6	2134.4	**1652.0**
21	538.2	973.4	**755.8**	1232.0	2246.8	**1739.4**
22	576.0	1036.8	**806.4**	1288.8	2362.0	**1825.4**
23	610.1	1102.2	**856.2**	1346.9	2470.1	**1908.5**
24	645.2	1162.8	**904.0**	1398.8	2580.6	**1989.7**
25	676.0	1225.0	**950.5**	1459.2	2683.2	**2071.2**
26	712.9	1288.8	**1000.9**	1513.2	2787.8	**2150.5**
27	745.3	1354.2	**1049.8**	1560.3	2883.7	**2222.0**
28	778.4	1413.8	**1096.1**	1616.0	2981.2	**2298.6**
29	812.3	1474.6	**1143.4**	1664.6	3080.3	**2372.4**
30	841.0	1536.6	**1188.8**	1714.0	3181.0	**2447.5**

Figure 5.1 (Continued) Variances as a function of numbers of subset and iteration.

Iteration Number	Subset = 6			Subset = 10		
	Left	Right	Average	Left	Right	Average
1	32.5	**46.2**	39.4	68.9	121.0	**94.9**
2	75.7	**141.6**	108.7	210.3	376.4	**293.3**
3	151.3	**282.2**	216.8	388.1	691.7	**539.9**
4	243.4	**445.2**	344.3	571.2	1017.6	**794.4**
5	346.0	**620.0**	483.0	750.8	1354.2	**1052.5**
6	453.7	**806.6**	630.1	924.2	1689.2	**1306.7**
7	561.7	**992.3**	777.0	1089.0	2007.0	**1548.0**
8	665.6	**1176.5**	921.1	1239.0	2323.2	**1781.1**
9	767.3	**1369.0**	1068.1	1391.3	2611.2	**2001.3**
10	870.3	**1552.4**	1211.3	1528.8	2894.4	**2211.6**
11	967.2	**1738.9**	1353.1	1664.6	3158.4	**2411.5**
12	1062.8	**1918.4**	1490.6	1789.3	3410.6	**2599.9**
13	1156.0	**2088.5**	1622.2	1918.4	3636.1	**2777.3**
14	1246.1	**2265.8**	1755.9	2034.0	3856.4	**2945.2**
15	1332.3	**2430.5**	1881.4	2143.7	4070.4	**3107.1**
16	1421.3	**2590.8**	2006.1	2256.3	4264.1	**3260.2**
17	1497.7	**2745.8**	2121.7	2362.0	4435.6	**3398.8**
18	1584.0	**2894.4**	2239.2	2460.2	4610.4	**3535.3**
19	1664.6	**3036.0**	2350.3	2560.4	4774.8	**3667.6**
20	1738.9	**3181.0**	2459.9	2652.3	4928.0	**3790.1**
21	1814.8	**3306.3**	2560.5	2745.8	5069.4	**3907.6**
22	1883.6	**3434.0**	2658.8	2840.9	5212.8	**4026.9**
23	1962.5	**3564.1**	2763.3	2926.8	5343.6	**4135.2**
24	2025.0	**3684.5**	2854.7	3003.0	5461.2	**4232.1**
25	2097.6	**3794.6**	2946.1	3091.4	5580.1	**4335.7**
26	2162.3	**3906.3**	3034.3	3169.7	5700.3	**4435.0**
27	2227.8	**4019.6**	3123.7	3249.0	5806.4	**4527.7**
28	2294.4	**4121.6**	3208.0	3317.8	5913.6	**4615.7**
29	2362.0	**4212.0**	3287.0	3398.9	6006.3	**4702.6**
30	2420.6	**4316.5**	3368.6	3469.2	6115.2	**4792.2**

Table 5.1 (Continued) Variances as a function of numbers of subset and iteration.

Iteration Number	Subset = 12			Subset = 20			Subset = 30		
	Left	Right	Average	Left	Right	Average	Left	Right	Average
1	84.6	148.8	**116.7**	265.7	462.3	**364.0**	392.0	806.6	**599.3**
2	269.0	462.3	**365.6**	670.8	1169.6	**920.2**	888.0	1857.6	**1372.8**
3	492.8	823.7	**658.3**	1036.8	1883.6	**1460.2**	1339.6	2766.8	**2053.2**
4	712.9	1197.2	**955.0**	1361.6	2550.3	**1955.9**	1730.6	3492.8	**2611.7**
5	924.2	1576.1	**1250.1**	1656.5	3136.0	**2396.2**	2088.5	4070.4	**3079.5**
6	1122.3	1936.0	**1529.1**	1918.4	3660.3	**2789.3**	2401.0	4542.8	**3471.9**
7	1310.4	2275.3	**1792.9**	2162.3	4121.6	**3141.9**	2683.2	4942.1	**3812.7**
8	1490.0	2601.0	**2045.5**	2381.4	4529.3	**3455.4**	2948.5	5299.8	**4124.2**
9	1656.5	2905.2	**2280.9**	2590.8	4886.0	**3738.4**	3181.0	5610.0	**4395.5**
10	1814.8	3181.0	**2497.9**	2777.3	5198.4	**3987.9**	3398.9	5898.2	**4648.6**
11	1962.5	3445.7	**2704.1**	2959.4	5490.8	**4225.1**	3600.0	6162.3	**4881.1**
12	2106.8	3684.5	**2895.7**	3124.8	5745.6	**4435.2**	3794.6	6400.0	**5097.3**
13	2246.8	3906.3	**3076.5**	3283.3	5975.3	**4629.3**	3969.0	6642.3	**5305.6**
14	2381.4	4108.8	**3245.1**	3434.0	6193.7	**4813.8**	4121.6	6855.8	**5488.7**
15	2510.0	4303.4	**3406.7**	3576.0	6400.0	**4988.0**	4277.2	7056.0	**5666.6**
16	2631.7	4475.6	**3553.7**	3708.8	6593.4	**5151.1**	4422.3	7259.0	**5840.6**
17	2745.8	4651.2	**3698.5**	3844.0	6773.3	**5308.6**	4569.8	7447.7	**6008.7**
18	2862.3	4802.5	**3832.4**	3969.0	6938.9	**5453.9**	4692.3	7621.3	**6156.8**
19	2970.3	4956.2	**3963.2**	4083.2	7106.5	**5594.9**	4816.4	7796.9	**6306.6**
20	3080.3	5083.7	**4082.0**	4199.0	7259.0	**5729.0**	4928.0	7956.6	**6442.3**
21	3181.0	5227.3	**4204.1**	4303.4	7396.0	**5849.7**	5041.0	8118.0	**6579.5**
22	3283.3	5343.6	**4313.5**	4409.0	7551.6	**5980.3**	5155.2	8281.0	**6718.1**
23	3375.6	5476.0	**4425.8**	4515.8	7691.3	**6103.6**	5256.3	8427.2	**6841.7**
24	3469.2	5580.1	**4524.7**	4610.4	7814.6	**6212.5**	5343.6	8556.3	**6949.9**
25	3564.1	5700.3	**4632.2**	4706.0	7938.8	**6322.4**	5446.4	8704.9	**7075.7**
26	3648.2	5806.4	**4727.3**	4802.5	8064.0	**6433.3**	5535.4	8836.0	**7185.7**
27	3733.2	5898.2	**4815.7**	4886.0	8190.3	**6538.1**	5610.0	8968.1	**7289.1**
28	3819.2	6006.3	**4912.7**	4970.3	8299.2	**6634.7**	5700.3	9082.1	**7391.2**
29	3893.8	6099.6	**4996.7**	5055.2	8408.9	**6732.1**	5776.0	9216.0	**7496.0**
30	3981.6	6193.7	**5087.7**	5126.6	8519.3	**6822.9**	5852.3	9331.6	**7591.9**

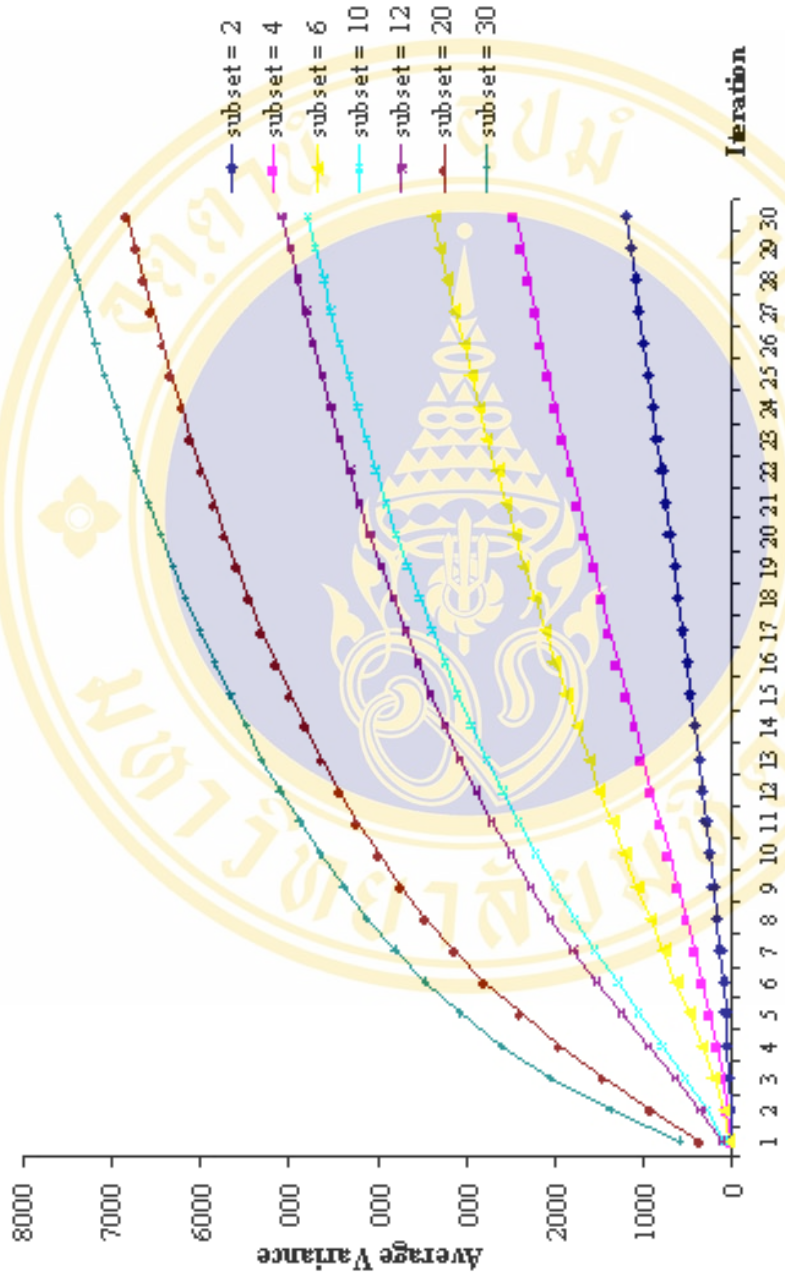

Figure 5.3 Variance plotted against iteration number of OSEM at different numbers of subset.

5.2 The Optimal Subset and Iteration Number of OSEM

In this section, we studied the optimal numbers of subset and iteration of OSEM algorithm. Figure 5.4 shows the true image (left) and the showed reconstructed image (slice 59) with 6 subsets and 2 iterations. The MSE was used to determine the differences between reconstructed images and true images. Table 5.2 reported the MSE with various numbers of subset and iteration.

Figure 5.5 (a) and (b) showed the plots between average MSE and iteration number at different numbers of subset. The results showed that 6 subset with 2 iterations and 2 subsets with 6 iterations gave the minimum MSE (0.01 and 0.03 respectively). Then computation times were observed and the results showed that the 6 iterations with 2 subsets and the 2 iterations with 6 subsets consumed 1.45 and 0.51 seconds respectively. Therefore, the 2 iterations with 6 subsets was selected.

(a) (b)

Figure 5.4 Brain phantom images. (a) True image and (b) reconstructed image using OSEM with 2 iterations at 6 subsets.

Table 5.2 The MSE as a function of numbers of subset and iteration.

Iteration Number	Subset = 2			Subset = 4		
	Left	**Right**	**Average**	**Left**	**Right**	**Average**
1	22.56	23.23	**22.90**	6.86	7.84	**7.35**
2	6.97	7.73	**7.35**	0.50	1.10	**0.80**
3	2.13	2.82	**2.48**	0.01	0.08	**0.04**
4	0.53	1.02	**0.78**	0.24	0.02	**0.13**
5	0.06	0.31	**0.19**	0.48	0.16	**0.32**
6	0.01	0.05	**0.03**	0.61	0.29	**0.45**
7	0.10	0.00	**0.05**	0.71	0.40	**0.55**
8	0.23	0.04	**0.14**	0.77	0.46	**0.62**
9	0.36	0.12	**0.24**	0.81	0.52	**0.66**
10	0.46	0.19	**0.33**	0.86	0.56	**0.71**
11	0.55	0.27	**0.41**	0.90	0.59	**0.75**
12	0.61	0.35	**0.48**	0.96	0.62	**0.79**
13	0.66	0.40	**0.53**	1.00	0.66	**0.83**
14	0.69	0.45	**0.57**	1.04	0.67	**0.86**
15	0.72	0.49	**0.61**	1.10	0.69	**0.90**
16	0.76	0.53	**0.64**	1.14	0.71	**0.93**
17	0.77	0.56	**0.67**	1.21	0.72	**0.97**
18	0.79	0.58	**0.68**	1.25	0.74	**1.00**
19	0.81	0.61	**0.71**	1.32	0.76	**1.04**
20	0.83	0.62	**0.73**	1.37	0.77	**1.07**
21	0.76	0.72	**0.74**	1.37	0.86	**1.12**
22	0.77	0.76	**0.77**	1.44	0.88	**1.16**
23	0.79	0.77	**0.78**	1.49	0.88	**1.19**
24	0.81	0.79	**0.80**	1.37	0.90	**1.14**
25	0.83	0.81	**0.82**	1.44	0.90	**1.17**
26	0.76	0.83	**0.79**	1.49	0.92	**1.21**
27	0.77	0.76	**0.77**	1.37	0.92	**1.15**
28	0.79	0.77	**0.78**	1.44	0.86	**1.15**
29	0.81	0.79	**0.80**	1.49	0.88	**1.19**
30	0.83	0.81	**0.82**	1.37	0.88	**1.13**

Figure 5.2 (Continued) The MSE as a function of numbers of subset and iteration.

Iteration Number	Subset = 6			Subset = 10		
	Left	Right	Average	Left	Right	Average
1	2.19	2.50	**2.34**	0.07	0.44	**0.25**
2	0.00	0.02	**0.01**	0.35	0.14	**0.25**
3	0.24	0.16	**0.20**	0.55	0.45	**0.50**
4	0.44	0.41	**0.42**	0.61	0.61	**0.61**
5	0.53	0.56	**0.55**	0.69	0.71	**0.70**
6	0.59	0.64	**0.62**	0.76	0.77	**0.77**
7	0.66	0.71	**0.68**	0.85	0.85	**0.85**
8	0.71	0.74	**0.72**	0.94	0.88	**0.91**
9	0.76	0.77	**0.77**	1.04	0.92	**0.98**
10	0.83	0.79	**0.81**	1.12	0.96	**1.04**
11	0.90	0.81	**0.86**	1.21	0.98	**1.10**
12	0.96	0.83	**0.89**	1.30	1.00	**1.15**
13	1.04	0.85	**0.94**	1.37	1.02	**1.19**
14	1.10	0.86	**0.98**	1.46	1.02	**1.24**
15	1.17	0.88	**1.03**	1.51	1.04	**1.28**
16	1.23	0.88	**1.06**	1.59	1.04	**1.31**
17	1.30	0.90	**1.10**	1.66	1.04	**1.35**
18	1.37	0.90	**1.14**	1.72	1.06	**1.39**
19	1.44	0.92	**1.18**	1.77	1.06	**1.41**
20	1.49	0.92	**1.21**	1.82	1.06	**1.44**
21	1.37	0.96	**1.16**	1.74	1.14	1.44
22	1.46	0.98	**1.22**	1.74	1.21	1.48
23	1.51	1.00	**1.26**	1.74	1.25	1.50
24	1.59	1.02	**1.30**	2.02	1.32	1.67
25	1.49	1.02	**1.25**	2.04	1.37	1.71
26	1.49	1.04	**1.26**	2.06	1.40	1.73
27	1.66	1.04	**1.35**	2.08	1.44	1.76
28	1.72	1.04	**1.38**	2.10	1.49	1.79
29	1.77	1.06	**1.41**	2.12	1.58	1.85
30	2.19	1.06	**1.44**	2.14	1.60	1.87

Table 5.2 (Continued) The MSE as a function of numbers of subset and iteration.

Iteration Number	Subset = 12			Subset = 20			Subset = 30		
	Left	**Right**	**Average**	**Left**	**Right**	**Average**	**Left**	**Right**	**Average**
1	0.04	0.08	**0.06**	1.54	0.07	**0.80**	1.42	0.35	**0.88**
2	0.76	0.94	**0.85**	1.10	0.79	**0.95**	0.29	0.72	**0.51**
3	1.04	1.30	**1.17**	1.14	1.12	**1.13**	0.64	0.37	**0.51**
4	1.23	1.42	**1.32**	1.32	1.37	**1.35**	0.86	0.79	**0.83**
5	1.44	1.49	**1.46**	1.54	1.56	**1.55**	1.02	0.85	**0.93**
6	1.66	1.54	**1.60**	1.74	1.69	**1.72**	1.10	0.88	**0.99**
7	1.85	1.59	**1.72**	1.93	1.80	**1.86**	1.17	0.90	**1.03**
8	2.04	1.61	**1.83**	2.07	1.85	**1.96**	1.21	0.92	**1.07**
9	2.22	1.64	**1.93**	2.22	1.90	**2.06**	1.25	0.94	**1.10**
10	2.37	1.66	**2.02**	2.34	1.96	**2.15**	1.30	0.96	**1.13**
11	2.53	1.69	**2.11**	2.46	1.99	**2.23**	1.35	0.98	**1.16**
12	2.66	1.72	**2.19**	2.56	2.02	**2.29**	1.39	1.00	**1.20**
13	2.79	1.74	**2.27**	2.66	2.04	**2.35**	1.42	1.02	**1.22**
14	2.89	1.74	**2.32**	2.72	2.04	**2.38**	1.44	1.04	**1.24**
15	2.96	1.77	**2.36**	2.79	2.07	**2.43**	1.49	1.06	**1.27**
16	3.06	1.77	**2.42**	2.86	2.10	**2.48**	1.51	1.08	**1.30**
17	3.10	1.80	**2.45**	2.92	2.10	**2.51**	1.54	1.10	**1.32**
18	2.79	1.80	**2.29**	2.99	2.13	**2.56**	1.56	1.12	**1.34**
19	2.86	1.80	**2.33**	3.06	2.13	**2.60**	1.59	1.14	**1.37**
20	2.92	1.82	**2.37**	3.10	2.16	**2.63**	1.59	1.17	**1.38**
21	3.10	2.02	**2.56**	2.79	2.22	**2.50**	1.74	1.46	**1.60**
22	2.79	2.04	**2.42**	2.86	2.34	**2.60**	1.74	1.51	**1.63**
23	2.86	2.02	**2.44**	2.92	2.46	**2.69**	2.02	1.59	**1.80**
24	2.92	2.02	**2.47**	3.35	2.56	**2.95**	2.04	1.66	**1.85**
25	3.10	2.02	**2.56**	3.13	2.66	**2.89**	2.02	1.72	**1.87**
26	2.79	2.02	**2.40**	3.20	2.72	**2.96**	2.02	1.77	**1.89**
27	2.86	2.02	**2.44**	3.28	2.79	**3.03**	2.02	1.82	**1.92**
28	2.92	2.04	**2.48**	3.35	2.86	**3.10**	2.02	1.74	**1.88**
29	3.13	2.02	**2.57**	3.13	2.92	**3.03**	2.31	1.74	**2.03**
30	3.20	2.02	**2.61**	3.20	2.99	**3.10**	3.31	1.74	**2.53**

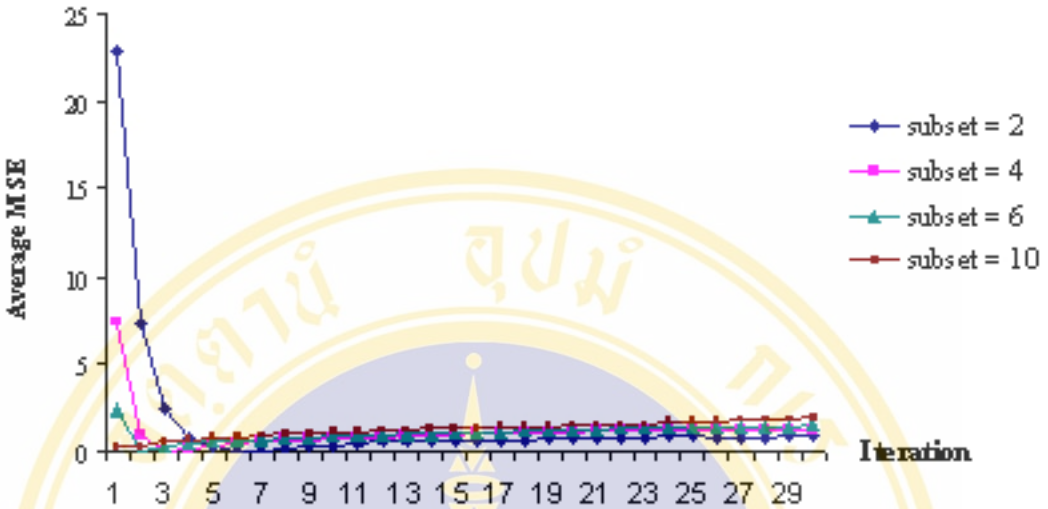

(a)

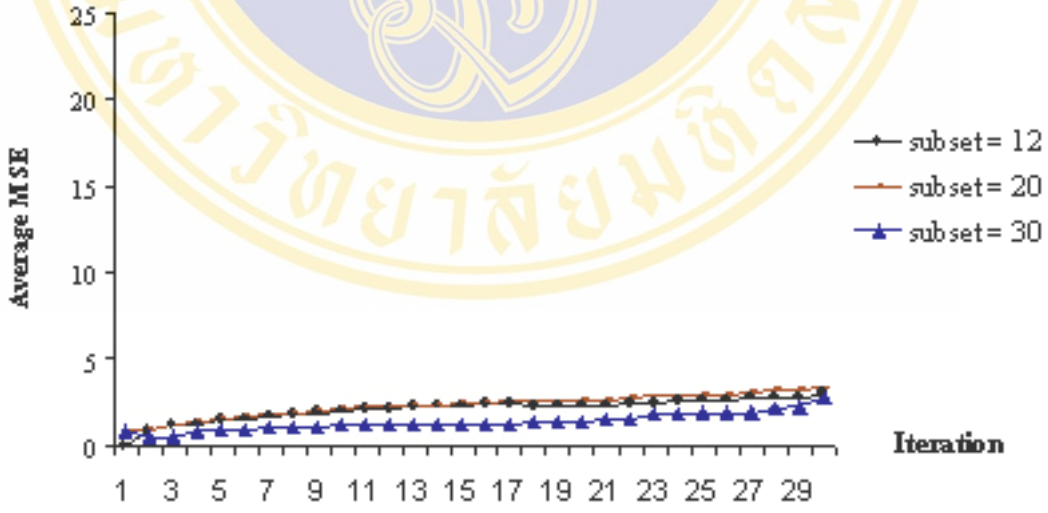

(b)

Figure 5.5 MSE plotted against iteration number of OSEM at different numbers of subset.

5.3 Preference Study

Table 5.3 showed frequencies of the scores obtained from two readers. The results showed that reader 1 preferred image B (OSEM algorithm) to image A (FBP algorithm) with 65.6 % (63 images of 96 images) and there was no difference between image A and B with 15.6 % (15 images of 96 images) and image A was better than image B with 18.8 % (18 images of 96 images). While reader 2 absolutely preferred image B to image A with 100 %.

Table 5.3 Frequency of the score

Reader	**Reader Preferences.**		
	Image A	**Image A = B**	**Image B**
1	18 images (18.8 %)	15 images (15.6 %)	65 images (65.6 %)
2	0 (0 %)	0 (0 %)	96 images (100 %)

CHAPTER VI
DISCUSSION AND CONCLUSION

6.1 Discussion

In our study, we studied the noise properties and the optimal subset and iteration numbers using the brain phantom. We found that the image noise in term of variance increased when the numbers of subset and iteration increased. These results agreed with previous studies. (5, 10, 11, 20, 25, 26)

To optimize numbers of subsets and iteration, we found that 2 iterations and 6 subsets gave minimum MSE, therefore these numbers are optimal. Then optimal parameters of OSEM were implemented for bone SPECT images. We used physician's preference study to evaluate OSEM algorithm compared with FBP algorithm. We found that one reader totally preferred OSEM algorithm to FBP algorithm because OSEM gave image quality with high resolution and without streak artifacts. While another reader preferred OSEM algorithm to FBP algorithm with 65.6 %. There were no differences between two algorithms with 15.6 % because the abnormalities were clearly and equally seen by two algorithms. This reader also preferred FBP algorithm to OSEM algorithm with 18.8 % because the reader thought that the image quality of OSEM was too good. That means the training sets of images are not sufficient for readers to get familiar with OSEM images.

6.2 Conclusion

The image noise obtained from OSEM iterative reconstruction increases as numbers of iteration and subset increase. The optimal numbers of iteration and subset are 2 and 6 respectively. Image quality of OSEM is superior to that of FBP for bone SPECT imaging.

6.3 Contribution of This Study

The major contribution of this study is the demonstration of the superiority of the OSEM iterative algorithm. We confirm that the image quality of OSEM algorithm for bone SPECT is better than that of FBP algorithm. Another contribution is the image reconstruction software. At the time we started this study there was none commercial image reconstruction software available in Thailand because it is very expensive. Another reason is nuclear medicine physician lacks knowledge of iterative algorithm even though they would like to improve image quality of SPECT images. Consequently, we used IDL to develop software for image reconstruction mainly in nuclear medicine. Although our software still needs further development, it can be used as a research tool or for academic purposes. In future work, we will expand the software to cover on medical image processing.

REFERENCES

1. Ahluwalia BD, editor. Tomographic methods in nuclear medicine: physical principles, instruments and clinical applications. Florida (FL): CRC Press; 1989:3 – 33.
2. Steve AM, editor. Review of nuclear medicine technology. 2th ed. Reston: Society of Nuclear Medicine;1996.
3. Keith J, Alex J B. The Whole brain atlas. Harvard Medical School. Availabel from: URL:http://www.med.hardvard.edu/AANLB/home.html
4. Bruyant PP. Analytical and iterative reconstruction algorithm in SPECT. *J Nucl Med* 2002; 43:1343-1358.
5. Hye KS, Mi J Y, Tae JJ, Dong OK, Jong-Doe L, Hyung SY, and others. ROC analysis of ordered subset expectation maximization and filtered backprojection technique for FDG-PET in lung cancer", *IEEE Nucl Sci Sym* 2001; 4:1801-1805.
6. Kohli V, King MA, Tin-Su P,Glick SJ. Compensation for distance-dependent resolution in cardiac-perfusion SPECT: impact on uniformity of wall counts and wall thickness. *IEEE Trans Nucl Sci* 1998;45(3):1104-1110.
7. Pieper BC, Bowsher JE, Torrnai MP, Archer CN, Jaszczak RJ. Parallel-beam tilted-head analytical SPECT reconstruction derivation and comparison with OSEM. *IEEE Tran Nucl Sci* 2002;49(5):2394-2400.
8. Pretorius PH, Gifford HC, Narayanan MV, King MA. Comparison of detection accuracy of perfusion defects in SPECT for different reconstruction strategies using polar map quantization. *IEEE Tran Nucl Sci* 2003;50(5):1569-1574.
9. Trotter DEG, Bowsher JE, Jaszczak RJ. Absoluter quantization of a spherical I-131 activity distribution using a high-resolution rotating collimator: a phantom study. *IEEE Tran Nucl Sci* 1999;48(1):65-73.

10. Cliff XW, Wesley ES, Griff B, Pete S. Performance evaluation of filtered backprojection reconstruction and iterative reconstruction methods for PET images. *J Comp Bio Med* 1998;28:13-25.
11. Didier B, Alain S, Niculaie P, Andre S. Maximum-likelihood reconstruction with ordered subsets in bone SPECT. IEEE Nucl Med Sci 1999:40:1978-1984.
12. Herman GT, Odhner D. Performance evaluation of an iterative image reconstruction algorithm for PET. *IEEE Trans Med Img* 1991;40(4):1198-1203.
13. CardioSPECT VMAX. Available from: URL: http://www.medcompare.com
14. Powsner RA and Pownsner ER. Essential of nuclear medicine physics. USA Blackwell Science;1998.
15. SPECT nuclear Imaging camera: cardiotroracic Imaging. Yale University of Medicine. Available from: URL: http://info.med.yale.edu
16. Bendriem B, Townsend DW. The theory and practical of 3D PET. Kluwer , Netherlands: Academic Publishers;1998.
17. Vandenberghe S, Asseler YD, Van WR, Kauppinen T, Koole M, Bouwents, and others. Iterative reconstruction algorithms in nuclear medicine. *J Comp Med Img* 2001;25:105-111.
18. Lange K, Carson R. EM reconstruction algorithm for emission and transmission tomography. *J Comp Assist Tomogr* 1984;8:306-316.
19. Hudson HM. Larkin R. Accerated image reconstruction using ordered subsets of projection data. *IEEE Trans Med Img* 1999;13:601-609.
20. Soo CL, Bruce HH, Keenan B, Thomas FL. Noise propagation in SPECT image reconstructed using an iterative maximum-likelihood algorithm. *Phys Med Bio* 1993;38:1713-1726.
21. Tsui BMW, Xide Z. Practical iterative reconstruction methods for quantitative cardiac SPECT image reconstruction. *IEEE Nucl Med Img* 1992;41(1):25-31.
22. Using IDL Manual. n.p.: Research System: 1999.
23. Building IDL Manual. n.p.: Research System: 1999.
24. Zubal G, Gindi G, Lee M, Harrell H, Smith E. High resolution anthropomorphic phantom for monte carlo analysis of internal radiation sources. 3rd Annual IEEE Symposium on Computer-Based Medical Systems. Chapel Hill, NC June 3-6, 1990;540-546.

25. Kadrmas DJ. Statistically regulated and adaptive EM reconstruction for emission computed tomography. *IEEE Trans Nucl Sci* 2001;48:790-798

26. Mustafovic S, Thielemans K, Hogg D, Bloomfiels P. Object dependency of resolution and convergence rate in OSEM with filtering. *IEEE Nucl Sci Sym* 2001;3:1786-1790

BIOGRAPHY

NAME	MR. Surachai Ngamratanapaiboon
DATE OF BIRTH	20 September 1977.
PLACE OF BIRTH	Samut Sakhon, Thailand
INSTITUTIONS ATTENDED	Mahidol University, 1996-2000 Bachelor of Science (Pharmacy) Mahidol University, 2001-2004 Master of Engineering (Biomedical Engineering)
POSITION & OFFICE	-
HOME ADDRESS	1094/73 T. Mahachai. A. Maeung Samut Sakhon 74000 Tel. 034-422797, 01-9812836 E-mail : mu20919@gmail.com